JMEPEG (2011) 20:489–496
DOI: 10.1007/s11665-011-9872-9

1059-9495/$19.00

Design of a Telescopic Linear Actuator Based on Hollow Shape Memory Springs

Andrea Spaggiari, Igor Spinella, and Eugenio Dragoni

(Submitted May 5, 2010; in revised form February 1, 2011)

Shape memory alloys (SMAs) are smart materials exploited in many applications to build actuators with high power to mass ratio. Typical SMA drawbacks are: wires show poor stroke and excessive length, helical springs have limited mechanical bandwidth and high power consumption. This study is focused on the design of a large-scale linear SMA actuator conceived to maximize the stroke while limiting the overall size and the electric consumption. This result is achieved by adopting for the actuator a telescopic multi-stage architecture and using SMA helical springs with hollow cross section to power the stages. The hollow geometry leads to reduced axial size and mass of the actuator and to enhanced working frequency while the telescopic design confers to the actuator an indexable motion, with a number of different displacements being achieved through simple on-off control strategies. An analytical thermo-electro-mechanical model is developed to optimize the device. Output stroke and force are maximized while total size and power consumption are simultaneously minimized. Finally, the optimized actuator, showing good performance from all these points of view, is designed in detail.

Keywords analytical modeling, hollow helical springs, linear actuator, quality function deployment, shape memory alloys

1. Introduction

Shape memory alloys are smart materials successfully exploited in the field of the actuation and of the microactuation, because of their high power/mass and force/mass ratios (Ref 1). On the one hand, SMA wires ensure a high actuating force, a minimal amount of needed active material and good operating frequency but they are undermined by poor strokes and considerable length of the overall construction (Ref 2). On the other hand, SMA helical springs grants high strokes per unit length of the actuator, but only for limited bandwidth (Ref 3) and exploiting much more active material.

Although a lot of SMA devices have been studied to overcome these limitations (Ref 4), a SMA actuator able to compete with conventional linear actuators has not been developed yet. The aim of this article is to design, optimize, and simulate the behavior of a high-performance SMA linear actuator with high stroke, high actuation force, high bandwidth, and minimal overall size. This result is achieved by designing the actuator according to a telescopic architecture, with concentric stages serially connected by sets of parallel helical SMA springs. The compact telescopic arrangement has the double advantage of generating a high stroke (given by the sum of the strokes of all the stages) while providing a high output force (given by the cumulative force of the spring set around each stage).

To further enhance the performance of the actuator, innovative hollow SMA springs previously studied by the authors (Ref 5, 6) are used to power up the stages. In comparison with conventional solid springs, the hollow spring construction allows the mass of the actuator to be reduced and its bandwidth to be increased dramatically.

A thermo-electro-mechanical model of the device has been developed and numerically optimized to maximize the specific power of the actuator. The result of the optimization has been the starting point of a detailed design of the final actuator. The SMA linear actuator developed in this section shows an excellent stroke (Δx = 165 mm), a high output force (F = 50 N), a good supply power (P = 106 W), and good total size (L_a = 252 mm, D_e = 111 mm). The whole system has been studied to be easy to assemble.

2. Conceptual Design

The conceptual design of the actuator has followed the Quality Function Deployment approach (Ref 7). The milestones of this approach are the House of Quality, the Functional Decomposition, the Concept Generation phase and, finally, the step of Concept Evaluation and Selection. The result of the Conceptual Design is a final concept, which is the best concept able to solve the problem of actuation exploiting the SMA. This section describes the above design phases and closes with a description of the selected concept.

This article is an invited paper selected from presentations at Shape Memory and Superelastic Technologies 2010, held May 16-20, 2010, in Pacific Grove, California, and has been expanded from the original presentation.

Andrea Spaggiari, Igor Spinella, and **Eugenio Dragoni**, Department of Engineering Science and Methods, University of Modena and Reggio Emilia, via Amendola, 2, 42122 Reggio Emilia, Italy. Contact e-mail: andrea.spaggiari@unimore.it.

List of symbols

A_h	Area of the hollow section spring, mm^2	M_f	Martensite finish temperature, °C
A_s	Austenite start temperature, °C	M_s	Martensite start temperature, °C
c_{AM}	Fictious transformation heat coefficient, W/mm^{2}K	M_t	Moment on the spring section, Nmm
C_h	Spring index of the hollow spring	n_s	Number of springs per set
C_s	Spring index of the solid spring	N_h	Number of active coils of the hollow springs
C^*	Dimensionless spring index	N_s	Number of active coils of the solid springs
d_{hi}	Inside diameter of the section of the hollow spring, mm	R	Electric resistance of the hollow spring, Ω
d_{ho}	Outside diameter of the section of the hollow spring, mm	R^*	Dimensionless electric resistance
d_s	Wire diameter of the solid spring, mm	t_c^*	Dimensionless cooling time
d^*	Dimensionless section diameter	t_r	Recovering time of the actuator, s
D_e	Maximum diameter of the actuator, mm	T_a	Ambient temperature, °C
D_h	Mean coil diameter of the hollow spring, mm	T_m	Maintenance temperature of the hollow springs, °C
D_s	Mean coil diameter of the solid spring, mm	T_p	Peak temperature of the hollow springs, °C
D^*	Dimensionless mean coil diameter	U	Volume of the actuator in closed configuration, l
E	Energy density of the actuator, mm	V_m	Maintenance voltage, V
F	Maximum force of the actuator, N	V_p	Peak voltage, V
F'	Force of a single hollow spring, N	W_h	Polar section modulus of the hollow section, mm^3
F_h	Maximum load on the spring, N	$\bar{X}$	Vector of the design variables
h	Coefficient of convection, W/mm^{2}K	α	Relative space between springs in each stage
J_h	Polar moment of inertia of the hollow section, mm^4	β	Coefficient for wound-coil prevention
K	Spring rate of the hollow spring, N/mm	Δx	Actuator stroke, mm
K_{ch}	Curvature correction factor of the hollow spring	ε	Coefficient for the frame of the actuator
K_{cs}	Curvature correction factor of the solid spring	γ	Shear strain
K^*	Dimensionless Curvature correction factor	ρ_e	Electric resistivity of the material, Ω mm
L_{tot}	Total length of the actuator in closed position, mm	ρ_m	Density of the material, kg/mm^3
L_a	Total length of the antagonist springs, mm	τ_h	Maximum shear stress of the hollow spring, MPa
L_0	Free length of the hollow spring, mm	τ_s	Maximum shear stress of the solid spring, MPa
m^*	Dimensionless spring mass	ξ	Void ratio of the hollow springs
M	Number of stages of the actuator		

2.1 House of Quality

Table 1 shows the complete House of Quality (HOQ) of the SMA actuator being designed. The House of Quality is a synthetic graphical instrument useful to show the customer needs (leftmost column), the related Metrics (uppermost row), the performances of the competitors (rightmost column), and the target specifications (lowermost row).

The customer needs were chosen to emphasize the size and the stroke requirements of the actuator. A set of metrics is associated with the customer needs, aimed at defining quantitative characteristics that help lead the design toward the achievement of the customer needs. The performances of the competitors were studied (regarding both customer needs and metrics) to define the target specification of the SMA actuator. The chosen competitor is a beam-based linear actuator based on SMA wires (Ref 4). This is one of the best microactuators in the field of SMA. This actuator ensures an extremely high ratio between actuation energy and volume. The actuation energy is defined as the product of the stroke of the actuator by its output force. The main drawbacks of the beam-based linear SMA actuator are the poor stroke, the poor force, and the absence of the bidirectionality.

The aim of this study is developing an actuator that must be competitive in the industrial field, with high stroke and high actuation force. The actuation energy will be reduced thanks to the hollow SMA spring concept, whose effectiveness has been proved in (Ref 5, 6).

Relevant target specifications reported in the HOQ in Table 1 are: total stroke higher than 150 mm, actuating force higher than 50 N, total length lower than 350 mm, external diameter lower than 100 mm, return time of the stem lower than 15 s.

2.2 Functional Decomposition

A complex design is typically simplified by breaking down the overall function of the product to simpler functions. The functional decomposition is effectively carried out by means of a functional diagram, which is a graphical representation of the critical functions of the system and of the existing relationships between these functions. Figure 1 shows the functional diagram of the SMA actuator. The diagram is focused on the analysis of the main critical function, which is "Convert Energy into Force."

2.3 Concept Generation

A concept generation stage process was exploited to find solutions to each critical function, and in particular to the main critical function "Convert Energy into Force." This process was undertaken by means of external research (to take inspiration from former solutions) and by means of internal research (to generate original ideas). For the internal generation of ideas, group-oriented techniques as brainstorming and the 6-3-5 method were used (Ref 7). A combination of the concept fragments led to a portfolio of global concepts.

2.4 Concept Evaluation and Selection

The final step is the evaluation and the selection of the concepts. This step was divided into three decisional steps: first,

Table 1 House of Quality

House of Quality		No	1	2	3	4	5	6	7	8	Competitors Beam-based SMAs actuator (Ref 4)
No	Customer needs	Metrics Weight	Diameter 5	Length 5	Density of energy 5	Stroke 5	Bidirectional 5	Time to come back 5	Nominal force 3	Electric Power 3	
1	Is compact	5	•	•	•						+
2	Gives high displacement	5			•	•					≀
3	Is bidirectional	5		o		o	•				⊥
4	Is fast	5						•			+
5	Gives high actuation forces	3			•		o		•		≀
6	Low power consumption	1								•	+
Units			mm	mm	Nm/dm^3	mm	Boolean	s	N	W	
Beam-based SMAs actuator (Ref 4)			17	30	31	2.5	No	3	4	1.4	
Target specifications			≤100	≤350	≥10	≥150	Yes	≤15	≥50	≤200	

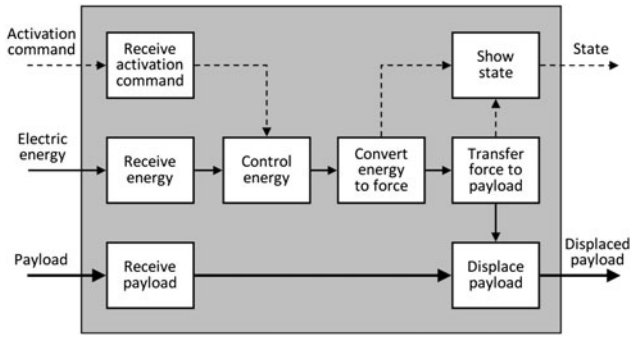

Fig. 1 Functional decomposition of the actuator

a screening matrix was used to choose the best three concepts; second, these concepts were critically reviewed and improved by analyzing their drawbacks; finally, the best concept was chosen exploiting a scoring matrix. Figure 2 shows the best concept that was identified for further development after this procedure. The concept is a linear telescopic actuator which will be described in the following section.

2.5 Concept Description

The actuator in Fig. 2 is formed by M concentric modules, arranged according to a telescopic architecture. Two antagonistic sets (S and S′) of SMA hollow helical springs, uniformly distributed around each stage, are used to power the stages. Starting from the center output stem (A), the concentric stages are connected in series by the SMA spring sets. This arrangement multiplies the total stroke Δx of the stem (A) and ensures a constant the output force (F) from stage to stage.

Figure 2(a) shows the actuator at rest, with no springs supplied and all the stages kept in an intermediate axial position. Heating of the upper sets of springs (S), as shown in Fig. 2(b), brings the stages in their uppermost position. Likewise, heating of the lower sets (S′) of springs as in Fig. 2(c) forces all the stages down to their lowermost position. Thus, the telescopic architecture easily grants a bi-directional device. The distance travelled by the output stem from the two limit positions defines the overall stroke Δx of the actuator.

Depending on the needs of the particular application, the concept in Fig. 2 allows both tension and compression SMA springs to be used as power elements. Because of the exploitation of hollow helical springs the actuator ensures the best compromise in terms of stroke, actuating force, and bandwidth of the system. The device is also easily controlled with a simple on-off logic and, provided that the M stages are supplied independently of each other, it can achieve a total of 3^M configurations and (at least) 2M + 1 different positions. This variety of configurations was not a specific target of the design but represents all the same an interesting feature of the system.

3. Modeling and Optimization

3.1 Thermo-Electro-Mechanical Model

A thermo-electro-mechanical model of the concept in Fig. 2 was developed. This model is useful to predict the behavior of

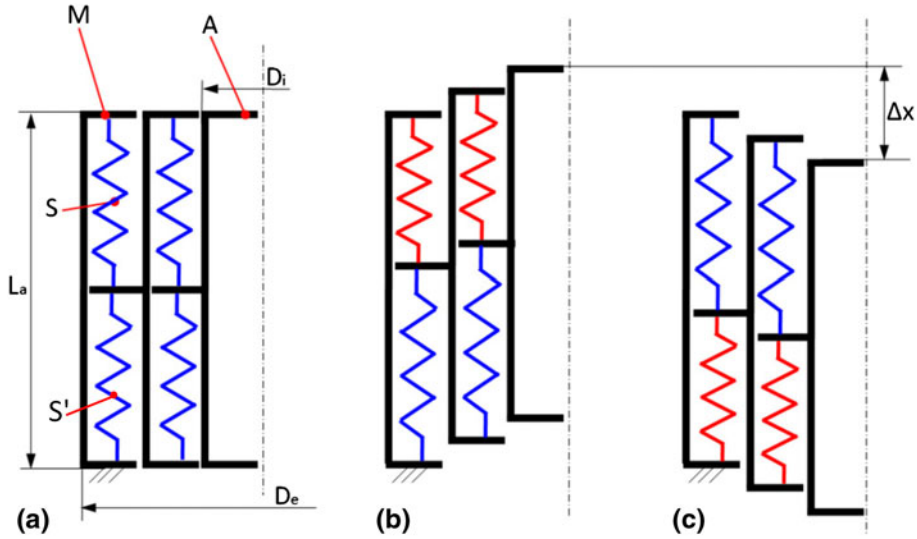

Fig. 2 Conceptual scheme of the telescopic architecture

the actuator. The model was then implemented in a numerical optimization software (see below) to reach an optimal configuration able to meet all the thermo-electro-mechanical constraints and at the same time to maximize the actuation energy for unit volume of the actuator.

The thermo-electro-mechanical model was built following the same line of thought used by the authors in Ref 3 for the simulation of an SMA rotary actuator. The design equations applying to the hollow springs are based on the theory developed in Ref 5 and validated in Ref 6. A summary of this theory is reported in appendix.

3.2 Position of the Optimization Problem

Formally, the optimization problem was stated as follows:

Find

$$\overline{X} = \{d_{ho}, \xi, C_h, N_h, L_o, L_a, M, n_s, V_m, V_p\} \quad \text{(Eq 1)}$$

so as

$$E\{\overline{X}\} = \max \quad \text{(Eq 2)}$$

subject to the design constraints listed below.

In (1) and (2), $\overline{X}$, is the vector of the design variables and $E(\overline{X}) = \frac{F\Delta x}{\text{Volume}}$ is the reference energy density of the actuator (where F is the maximum force of the actuator, Δx the stroke, and U the volume of the actuator in the closed configuration in Fig. 2(a).

Vector $\overline{X}$ includes the following variables: the outside diameter, d_{ho}, of the section of the hollow springs; the void ratio, $\xi = \frac{d_{hi}}{d_{ho}}$, between inside diameter, d_{hi}, and the outside diameter of the spring cross section; the spring index, $C_h = \frac{D}{d_{ho}}$ (where D is the mean coil diameter of the springs); the number of active coils, N_h; the free length, L_0, of the hollow springs; the total length, L_a, of the antagonistic spring sets in each stage (Fig. 2); the number of stages, M; the number of SMA springs, n_s, in each spring set (S or S′); the peak supply voltage, V_p, and the maintenance voltage, V_m.

The design variables were subjected to the following mechanical, electric, and thermal constraints (see Fig. 2 and List of symbols).

Mechanical constraints:

$$\Delta x \geq \Delta x_{adm} \quad \text{(Eq 3)}$$

$$F \geq F_{adm} \quad \text{(Eq 4)}$$

$$L \leq L_{adm} \quad \text{(Eq 5)}$$

$$D_e \leq D_{adm} \quad \text{(Eq 6)}$$

$$n_s \leq \frac{\pi[D_i + \alpha d_{ho}(1 + C_h)]}{\alpha d_{ho}(1 + C_h)} \quad \text{(Eq 7)}$$

$$\gamma_{max} \leq \gamma_{adm} \quad \text{(Eq 8)}$$

Thermal constraints:

$$T_p \geq A_f \quad \text{(Eq 9)}$$

$$T_m \geq M_s \quad \text{(Eq 10)}$$

$$t_r \geq t_{adm} \quad \text{(Eq 11)}$$

Electrical constraints:

$$V_p \geq V_{adm} \quad \text{(Eq 12)}$$

From the mechanical standpoint, constraints (3) and (4) request a minimum stroke and a minimum admissible output force for the actuator. Constraints (5) and (6) limit the length and the outside diameter of the device. Constraint (7) ensures that the n_s springs around each stage are set apart, circumferentially, by a fraction α of the section diameter, d_{ho}). Finally, constraint (8) limits the maximum shear strain in the alloy below the admissible value.

On the thermal side, constraint (9) requires that the SMA springs are supplied with an electric peak tension, V_p, high enough to bring the alloy to the peak temperature, T_p, higher than the austenite finish temperature, A_f. Similarly, constraint

(10) implies that the maintenance temperature, T_m, of the springs is kept just above the martensite start temperature, M_s, of the alloy. As shown by the authors in Ref 3, this choice exploits the hysteresis of the alloy to increase the energetic efficiency of the actuator. Constraint (11) puts an upper limit to the pull-in time of the stem, t_r, used as a measure of the dynamic performance of the actuator.

Finally, the electric constraint (12) ensures that the peak voltage needed to supply the springs is lower than the available voltage.

3.3 Numerical Optimization

In order to carry out the numerical optimization it is convenient to write the equations for the objective function and the constraints which are not explicit in previous section 3.2.

The objective function is given by the ratio of actuator energy to the actuator volume

$$E_{tot} = F \cdot M \cdot \Delta x \qquad \text{(Eq 13)}$$

$$\text{Volume} = \pi L_a (D_i + (2Md_{ho}(C_h + 1)(1 + \alpha))^2 \qquad \text{(Eq 14)}$$

where the internal diameter $D_i = 20$ mm is needed to provide enough room to place the center through-rod.

The mechanical constraints given in the previous section can be expressed as

$$\Delta x = M\left(\frac{L_a}{2} - N_h d_{ho}(1 + \beta)\right) \qquad \text{(Eq 15)}$$

$$F = F' \cdot n_s \qquad \text{(Eq 16)}$$

$$L = L_a \varepsilon \qquad \text{(Eq 17)}$$

$$D_e = D_i + (2Md_{ho}(C_h + 1)(1 + \alpha)) \qquad \text{(Eq 18)}$$

where $\beta = 0.1$ is a coefficient used to prevent spring damage in the close-wound position, F' is the force given by a single hollow spring (see Appendix and Ref 5), $\varepsilon = 0.1$ is a coefficient which takes into account the room for the actuator frame. The explicit expression of the shear strain in a hollow SMA spring γ is provided in Ref 5 and not reported here for the sake of brevity.

The thermal and electrical constraints are expressed in terms of the design variables as well, considering that the resistance of the hollow spring R can be cast as a function of ξ

$$R = 4\rho_e \frac{C_h N_h}{d_{ho}(1 - \xi^2)} \qquad \text{(Eq 19)}$$

$$T_p = \frac{V_p^2}{R} \frac{1}{h \cdot (\pi d_{ho} \cdot \pi d_{ho} C_h n_s)} + T_a \qquad \text{(Eq 20)}$$

$$T_m = \frac{V_m^2}{R} \frac{1}{h \cdot (\pi d_{ho} \cdot \pi d_{ho} C_h n_s)} + T_a \qquad \text{(Eq 21)}$$

$$t_r = \frac{\rho_m}{4} d_{ho}(1 - \xi^2) \frac{c_{AM}}{h} \ln\left(\frac{M_s - T_a}{M_f - T_a}\right) \qquad \text{(Eq 22)}$$

where ρ_e is the electric resistivity of the SMA, h is coefficient of heat exchange under the hypothesis of purely convective cooling, T_a is the ambient temperature, ρ_m is the density of the material and c_{AM} the fictious transformation specific heat coefficient according to Ref 8.

The optimization task defined in the previous section was carried out numerically with the following values in the constraints (3-12): $\Delta x = 150$ mm, $F_{adm} = 50$ N, $L_{adm} = 350$ mm, $D_{adm} = 100$ mm, $\alpha_{adm} = 0.1$, $\gamma_{adm} = 0.015$ rad, $A_f = 58.4$ °C, $M_s = 24.7$ °C, $t_{adm} = 15$ s, $V_{adm} = 12$ V.

Before the numerical solution, the design choice was made to adopt the same cross section ($d_{hi} = 1$ mm, $d_{ho} = 1.3$ mm, $\xi = 0.77$) of the springs that the authors fabricated and tested successfully in Ref 6). This constraint ensured that the springs could actually be manufactured without any problems during winding of the tube (NiTi alloy supplied by SAES Getters) around the mandrel. The main difference in comparison with the spring described in Ref 6 is the spring index, which was reduced from $C_h = 9$ to $C_h = 6$ to reduce the size of the actuator.

The numerical optimization is carried out using commercial optimization software (Lingo, Lindo Systems, 1415 North Dayton Street, Chicago, USA). The solver take as inputs the constraints and the object function and returns the optimized set of variables which satisfies the problem using a feasible direction algorithm. The solution of the optimization problem gave the following optimum design vector:

$$\overline{X^*} = \left\{ \begin{array}{l} d_{ho} = 1.3 \text{ mm} \\ \xi = 0.77 \\ C_h = 6 \\ N_h = 70 \\ L_0 = 246 \text{ mm} \\ L_a = 320 \text{ mm} \\ M = 3 \\ n_s = 10 \\ V_m = 3 \text{ V} \\ V_p = 3.8 \text{ V} \end{array} \right\} \qquad \text{(Eq 23)}$$

which provides the maximum objective function $E = 2.42$ J/L.

4. Detailed Design

A detailed solid model design of the optimal actuator was made using SolidWorks system. Figure 3 shows longitudinal section views of the system in the rest position (Fig. 3a) and in the leftmost extended position (Fig. 3b).

A center through-rod (A) is showed in Fig. 3(a) together with three concentric stages (M_1, M_2, and M_3). The stages and the rod are connected together in series using compression hollow SMA springs (S). The spring ends are attached to the caps (T_1, T_2, and T_3), which are rigidly connected to the stages (M_1, M_2, and M_3) and to the circular plates (P_1, P_2, and P_3). The plates are rigidly connected to the rod (A) and to modules (M_1) and (M_2). Longitudinal spacers interposed between the springs ensure that the springs remain in the correct circumferential position. The spacers also support the springs against global elastic instability and provide a mechanical stop to prevent overstraining the SMA springs.

Electric contacts placed on the caps and on the plates provide the correct supply of the hollow SMA springs under the peak tension, $V_p = 3.8$ V, and the maintenance voltage, $V_m = 3$ V. The total number of SMA springs (S) is 60 (two

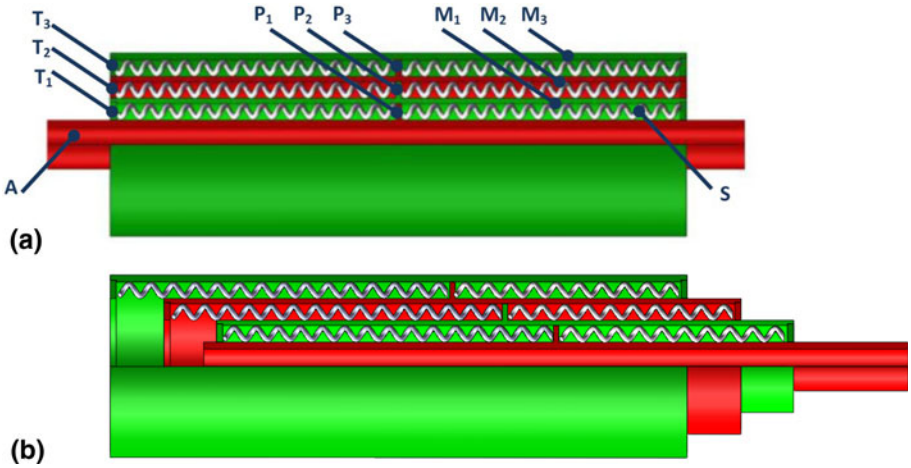

Fig. 3 Partial section of the actuator in closed position (a) and in extended position (b). Configuration (b) can be reversed symmetrically

sets of 10 springs for each of three stages). The total length of the actuator is 352 mm and the external diameter is 111 mm.

5. Discussion

The Discussion is focused on three points:

- performances of the telescopic actuator in comparison with the target specifications and other linear actuators, both SMA and conventional;
- advantages and drawbacks of the telescopic concept;
- future areas of investigation and possible improvements.

The target specifications related to the maximum dimensions of the actuator can be considered achieved: the length of the system is L_{tot} = 352 mm (slightly higher than the admissible length 350 mm) and the external diameter is D_e = 111 mm (11 mm more than the admissible external diameter). The stroke of the actuator is 165 mm, so it is higher than the target specification (150 mm) and the nominal force of 50.2 N matches the target specification of 50 N. The specific energy of the actuator is 2.42 J/L, slightly less than the target value of 2.5 J/L. The target cooling time is achieved and the electric power is 106 W, half than the target specification.

The comparison between the developed telescopic actuator and the beam-based SMA actuator in Table 1 shows that the proposed geometry enjoys higher strokes, although the specific energy is much lower. When compared with conventional linear actuators, the telescopic SMA actuator shows inferior performances, because of the intrinsic inefficiency of the shape memory alloys. Conventional electrical actuator may have efficiency above 90%, while traditional pneumatic actuators have specific energies higher than 50 J/L. Due to these drawbacks, this actuator can be considered and improvements only if compared with other SMAs actuators as in Ref 3, 4, but cannot yet compete successfully with other conventional electric actuators.

The main reason of the improvement over former SMA solutions is the exploitation of the hollow SMA springs. The hollow geometry can be thus considered a good way to increase the performances of SMA actuators, in particular, in terms of increased bandwidth, higher strokes, and greater actuating forces. As a drawback the SMA tubes not only cost more than SMA wires, but also the technology used to wind them on a mandrel is quite complex (Ref 6), especially when the void ratio is high (0.77), leading to much more expensive final active elements. The telescopic geometry, although featuring a lesser specific density than single-stage compliant geometries (springs or wires), provides an indexed positioning of the device by means of simple on-off activation of the stages. This feature could be further exploited by adding more modules to the system so as to achieve many discrete positions with no need for complex proportional control.

6. Conclusions

This article deals with the conceptual design, modeling, numerical optimization, and detailed design of a telescopic linear actuator based on hollow SMA springs. The use of the hollow spring construction and the telescopic architecture leads to excellent performances in comparison with other SMA actuators. By contrast, the performances of the actuator, especially in terms of maximum force and energy density, are still worse than other conventional electric linear actuators. A distinguished advantage of the telescopic SMA actuator lies in its ability to assume a set of discrete positions (indexation), easily achieved with simple on-off control schemes.

Appendix

Assumptions

To compare the performances of the hollow SMA spring with those of a solid-wire SMA spring, Spinella and Dragoni (Ref 5) assume that the two springs: (a) are made from the same material; (b) have the same spring index, C_h; (c) have the same spring rate, K; (d) undergo the same maximum load, F_h; (e) sustain the same maximum shear stress, τ_h. These conditions aim at designing the two springs (hollow and solid) with equivalent mechanical properties.

Design Variables

Geometrically, the hollow spring is defined by inner tube diameter, d_{hi}, outer tube diameter, d_{ho}, mean coil diameter, D_h, number of active coils, N_h. The solid spring is defined by wire diameter, d_s, mean coil diameter, D_s, number of active coils, N_s. In addition to these primary variables, two useful auxiliary variables that simplify the mathematical model are the spring indices, C_h and C_s, and the "void" ratio, ξ, defined as

$$C_h = \frac{D_h}{d_{ho}} \quad \text{(Eq 24a)}$$

$$C_s = \frac{D_s}{d_s} \quad \text{(Eq 24b)}$$

$$\xi = \frac{d_{hi}}{d_{ho}} \quad \text{(Eq 25)}$$

The void ratio, ξ, measures the hollowness of the section of the hollow spring. By definition, this parameter ranges from a minimum value of 0 (solid section) to a (theoretical) maximum value of 1 (vanishingly thin hollow section). By means of definition (25), the properties of the hollow spring are conveniently written with reference to the outer diameter, d_{ho}, of the cross section. For example, the area of the hollow section, $A_h = \pi\left(d_{ho}^2 - d_{hi}^2\right)/4$, can be recast as

$$A_h = \frac{\pi}{4} d_{ho}^2 \left(1 - \xi^2\right) \quad \text{(Eq 26)}$$

Similarly, the polar moment of inertia of the hollow section, $J_h = \pi\left(d_{ho}^4 - d_{hi}^4\right)/32$, can be written as

$$J_h = \frac{\pi}{32} d_{ho}^4 \left(1 - \xi^4\right) \quad \text{(Eq 27)}$$

from which the polar section modulus of the hollow section, $W_h = 2J_h/d_{ho}$, becomes

$$W_h = \frac{\pi}{16} d_{ho}^3 \left(1 - \xi^4\right) \quad \text{(Eq 28)}$$

Reference 5 presents the full list of hollow spring properties written with the format of Eq 3-5 and shows how the relative properties of mechanically equivalent hollow and solid springs can be expressed as dimensionless functions of the only void ratio, ξ. For the sake of example, two of these functions are addressed in the following sections, involving the outer section diameters and the number of active coils of the two springs.

Outer Section Diameters

The expression of the maximum shear stress in the hollow section is given by $\tau_h = K_{ch}(M_t/W_h)$, in which factor K_{ch} accounts for shear and curvature effects. Entering $M_t = F_h D_h/2$ and W_h given by (18), the maximum shear stress becomes

$$\tau_h = \frac{8F_h}{\pi} \cdot \frac{C_h}{d_{ho}^2\left(1 - \xi^4\right)} K_{ch} \quad \text{(Eq 29)}$$

The maximum shear stress in the solid spring, τ_s, produced by the same force F_h (assumption (d) above), is obtained from (29) by letting $\xi = 0$ and replacing subscript "h" with subscript "s." This gives

$$\tau_s = \frac{8F_h}{\pi} \cdot \frac{C_s}{d_s^2\left(1 - \xi^4\right)} K_{cs} \quad \text{(Eq 30)}$$

Equating (29) and (30) (see assumption (e) above) with $C_h = C_s$ (assumption (b) above) and recognizing that $K_{ch} \approx K_{cs}$ (Ref 5) leads to

$$\frac{d_{ho}}{d_s} = \frac{1}{\sqrt{1 - \xi^4}} \quad \text{(Eq 31)}$$

Number of Active Colis

Reasoning as in the previous section, the enforcement of the same spring rate in both springs (condition (c) above) gives the following relationship between the number of active coils of the two springs

$$\frac{N_h}{N_s} = \sqrt{1 - \xi^4} \quad \text{(Eq 32)}$$

Discussion

Table 2 collects most of the dimensionless functions developed in Ref 5 following the procedure shown above. Each function represents the ratio between a given property of the hollow spring and the corresponding property of the equivalent solid spring. For example, the curve labeled d^* gives the ratio $d^* = d_{ho}/d_s$ provided by Eq 21. Similarly, the curve labeled N^* gives the ratio $N^* = N_h/N_s$ defined by Eq 32. All the functions listed in Table 2 are plotted in Fig. 4 against the void ratio, ξ. The shaded area in Fig. 4 marks the range of void ratios ($\xi > 0.81$) that violate the buckling condition of the tube wall (Ref 5).

Figure 4 shows that for very low void ratios ($\xi \leq 0.1$) the properties of the hollow and the solid spring coincides (all dimensionless functions are close to 1). For increasing void ratios, characteristics K^* and C^* maintain the unit value (a necessary consequence of assumptions (b) and (c) above) while the other properties change remarkably. The only negative feature of the hollow spring is its greater transverse size, testified by the dimensionless section diameter (d^*) and mean coil diameter (D^*) rising above unity for $\xi > 0.4$. However,

Table 2 Summary of theoretical dimensionless spring properties comparing the performance of hollow and solid construction (data from Ref 5)

Dimensionless spring property	Symbol	Definition	Dimensionless function value
Void ratio	ξ	$\frac{d_{hi}}{d_{ho}}$	ξ
Wire diameter	d^*	$\frac{d_{ho}}{d_s}$	$\frac{1}{\sqrt{1-\xi^4}}$
Mean coil diameter	D^*	$\frac{D_h}{D_s}$	$\frac{1}{\sqrt{1-\xi^4}}$
Spring index	C^*	$\frac{C_h}{C_s}$	1
Spring rate	K^*	$\frac{K_h}{K_s}$	1
Number of active coils	N^*	$\frac{N_h}{N_s}$	$\sqrt{1-\xi^4}$
Mass of active coils	m^*	$\frac{m_{ha}}{m_{sa}}$	$\frac{1}{\sqrt{1-\xi^2}}$
Cooling time	t_c^*	$\frac{t_{hc}}{t_{sc}}$	$\sqrt{\frac{1-\xi^2}{1+\xi^2}}$
Electric resistance	R^*	$\frac{R_h}{R_s}$	$1-\xi^2$

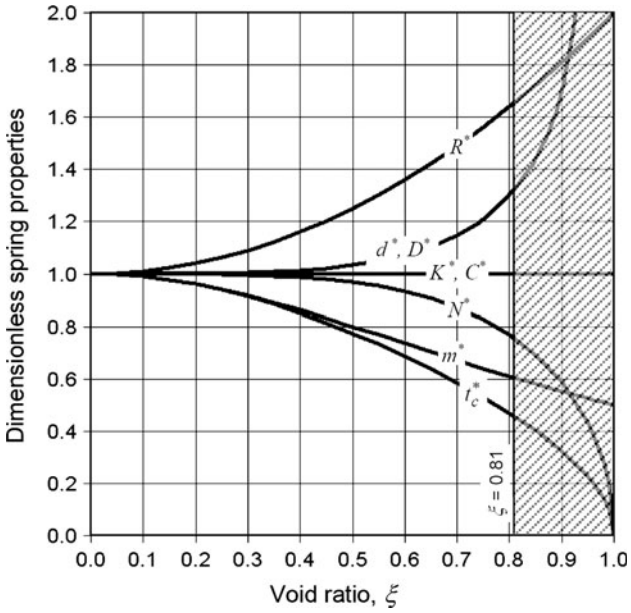

Fig. 4 Theoretical dimensionless properties of the hollow spring as a function of the void ratio (data from Ref 5)

within the range of allowable void ratios ($\xi \leq 0.81$) the relative increase is a mere 30% above the corresponding solid spring. In all other respects, the hollow spring outperforms the solid one. To begin with, the number of coils, N*, is reduced up to 25%, with slight benefits in terms of manufacturability. More important is the rapid increase observed in the electric resistance, R*, and the marked decrease shown by the spring mass, m*, and the cooling time, t_c^*, which bring the advantages described in the text. Reference 5 demonstrates that the hollow spring outperforms the solid spring also in terms of properties not shown in Fig. 4 (for example natural frequencies and buckling loads).

References

1. D. Mavroidis, C. Pfeiffer, M. Mosley, and U. Rutgers, *Conventional Motors, Shape Memory Alloys and ElectroRheological Fluids, Vol. 4 of The Topics on NDE (TONE) Series*, ASNT, Columbus, OH, 2000
2. I. Spinella and E. Dragoni, Design Equations for Binary Shape Memory Actuators Under Dissipative Forces, *J. Mech. Eng. Sci.*, 2009, **223**(C3), p 531–543
3. I. Spinella, G. Sciré Mammano, and E. Dragoni, Conceptual Design and Simulation of a Compact Shape Memory Actuator for Rotary Motion, *J. Mater. Eng. Perform.*, 2009, **18**(5), p 638–649
4. E.A. Khidir, N.A. Mohamed, M.J.M. Nor, and M.M. Mustafa, A New Concept of a Linear Smart Actuator, *Sens Actuators A*, 2007, **135**, p 244–249
5. I. Spinella and E. Dragoni, Analysis and Design of Hollow Helical Springs for Shape Memory Actuators, *J. Intell. Mater. Syst. Struct.*, 2010, **21**(2), p 185–199
6. I. Spinella, E. Dragoni, and F. Stortiero, Modelling, Prototyping and Testing of Helical Shape Memory Compression Springs with Hollow Cross-Section, *ASME J. Mech. Des.*, 2010, **132**(6), p 061008. doi: 10.1115/1.4001601
7. K.T. Ulrich and S.D. Eppinger, *Product Design and Development*, McGraw-Hill, Columbus, 2008
8. D. Reynaerts and H.V. Brussel, Design Aspects of Shape Memory Actuators, *Mechatronics*, 1998, **8**, p 635–656